nature

SUPPLEMENTARY INFORMATION

https://doi.org/10.1038/s41586-018-0646-5

In the format provided by the authors and unedited.

Dinosaur egg colour had a single evolutionary origin

Jasmina Wiemann[1]*, Tzu-Ruei Yang[2] & Mark A. Norell[3]

[1]Department of Geology & Geophysics, Yale University, New Haven, CT, USA. [2]Steinmann Institute for Geology, Mineralogy, and Paleontology, University of Bonn, Bonn, Germany. [3]Division of Vertebrate Paleontology, American Museum of Natural History, New York, NY, USA. *e-mail: jasmina.wiemann@yale.edu

Supplementary Note 1

Dinosaur egg colour had a single evolutionary origin

Jasmina Wiemann, Tzu-Ruei Yang, Mark A. Norell

Correspondence to: jasmina.wiemann@yale.edu

This Supplementary Note 1 includes:

Supplementary Figures 1-5
Supplementary Tables 1-2

1. Methods

a. Why Raman spectroscopy?

Bioanalytics can be performed in various different ways. Nuclear magnetic resonance (commonly H-NMR, or C-NMR) and single crystal X-ray diffraction (single-crystal XRD) offer information on the molecular structure, conformation, and higher order organization of a compound[33,34]. NMR and single crystal XRD are, however, destructive, and cannot be applied *in situ* to a fossil sample.

High-performance liquid chromatography (HPLC), or gas chromatography (GC), coupled to a mass spectrometer (MS) can provide information on the isomer composition, purity, and exact mass of a compound[35,36]. Exact mass determinations are an established tool for low-weight biomolecule identification, given exact knowledge of the molecular structure and weight of the compound targeted[35,36]. Thus, such MS methods can only be applied when we know what kind of compound we are looking for, and they only provide information on whether a detected compound has the same mass as the target compound – it is a presence/absence method[36]. As in the case of NMR and XRD, classic MS requires destructive sampling, but moreover, it requires successful extraction, and sufficient amounts of the target compound. Such classic MS routines cannot be applied *in situ* to a fossil, and thus cannot reveal spatial patterns in biomolecule distributions.

Derived, fragmentation-based MS methods, such as secondary ion MS ((ToF) SIMS), and matrix assisted laser absorption ionization imaging (MALDI Imaging), can provide *in situ* information on biomolecular compounds in a fossil (SIMS), but only allow small molecular fragments to be imaged (e.g. the amide function of a peptide) and therefore offer reduced "molecular resolution" (SIMS), or have not yet been applied to fossils (MALDI Imaging) [35,36].

A third, also target-based bioanalytical method is represented by immunological/enzymatic techniques. They rely on the highly specific interaction between antibodies and antigens/enzymes and substrates, which is based on characteristic molecular structures and superstructures exhibiting intermolecular interactions with their antibody/enzyme. Antibody-antigen/enzyme-substrate interactions require unaltered preservation of a target compound in the fossil, and they are also almost inevitably affected in their binding specificity by the *in situ* chemistry of fossil soft tissues[26,39,40], and the fossil-based salt and soluble fraction in *ex situ* assays. The specificity of antibody-antigen/enzyme-substrate binding in fossils has not been validated, and remains problematic. Based on previous work[26], diagenetic transformation of proteinaceous matter in fossil soft tissues yields N-rich heterocycles which are well known in medicine and food chemistry for their unspecific binding and defunctionalization of biomolecules, such as antibodies and enzymes[41].

Finally an upcoming method in bioanalytics is light spectroscopy. This non-destructive, *in situ* and *ex situ* applicable approach uses either infra-red light or monochromatic visible light to induce inelastic scattering[42,43]. The incoming light interacts with molecular vibrations in a fossil sample, shifting the wavelength of the emitted light either up or down[42]. These shifts produce characteristic patterns, which can be assigned to certain functional groups in a fossil sample of unknown composition – it is a fingerprinting method which does not require exact information on the target molecule[42]. Two complementary methods are infra-red spectroscopy and Raman spectroscopy[42]. Raman spectroscopy is a well-established tool, which allows molecular identification of an unknown, even impure or heterogenic fossil sample, in a non-destructive fashion, and provides spatial information on composition[43]. No extraction is required, the molecular resolution exceeds that of SIMS, and exposure times are in the range of a few seconds[43]. High-resolution point measurements on a fossil sample allow qualitative identification of preserved compounds, while surface maps and sample depth profiles (either in

a section or with a truly confocal Raman microspectroscope) can target the distribution of one or more compounds.

For studies on soft tissue/molecular preservation including samples with a huge variety of biomolecule degradation products (e.g. eggshell pigment degradation products), a high-molecular resolution, non-target-specific approach that does not require precise knowledge of a target compound, and has the potential to provide spatial information *in situ*, is the method of choice – Raman microspectroscopy.

b. Raman spectroscopic software

All spectra were acquired in Labspec 5[44] (spectral acquisition, mapping acquisition, standard spike removal) and subjected to a standard baseline correction (adaptive baseline, 50%, no offset, no smoothing) and standard normalization based on the highest band in each spectrum in SpectraGryph 1.2 spectroscopic software[45]. Whole spectra- and pigment fingerprint region-based Principal Component Analyses were performed in PAST 3[46].

c. Raman band assignments

All Raman band assignments (Supplementary Table 1) used in this study are based on our reevaluation of published Raman studies on avian eggshell pigments, proteinaceous matter and its degradation products, and lipids. We used Thomas et al. (2015)[30] and supplementary information as a guideline for band assignments of eggshell colour pigments[47,48,49]. However, our measurement routine provided a slightly increased band resolution (compare Fig. 1 to Thomas et al. 2015), so we reevaluated and refined all significant Raman bands. We define a significant signal as a Raman signal that has a band height at least three times the intensity of

the background noise, and shows up consistently. All our spectra were baselined and normalized; this does not affect the band positions.

We obtained a new set of fingerprint bands for both pigments, biliverdin (Bv) and protoporphyrin (PP); these show no correspondence with spectra for pigment-like protein fossilisation products (PFPs, see Chapter 1g). The results are listed below together with additional Raman band assignments for PFP, and for lipid remains that might be present[26]. Resulting differences to the egg colour pigment band assignments reported in Thomas et al. (2015)[30] are bands more diagnostic for Bv and PP (Supplementary Table 1). Bv is a linear tetrapyrrole and PP is a cyclic tetrapyrrole. Due to their lack of bilateral symmetry, both molecules give rise to a number of Raman bands representing different vibrational modes of their functional groups. The increased resolution of our Raman setup revealed more than seven[30] Raman bands diagnostic for Bv, and more than five[30] Raman bands diagnostic for PP (Supplementary Table 1). Among all bands detected for Bv and PP, nine differentiated Bv from PFPs, and thirteen differentiated PP from PFPs. Both pigments shared two diagnostic Raman bands at 1166 cm^{-1}, and 1557 cm^{-1} (Supplementary Table 1). Based on this increased subset of pigment fingerprint bands, the reliability of detection of the presence or absence of biliverdin and protoporphyrin is increased compared to previous Raman-based studies on eggshell pigments.

Over very short exposure times (2 – 5 s), the PP band at 1350 cm^{-1} Raman shift is still significant, leading us to select it for practical reasons for PP eggshell surface maps (for an explanation of the calibration and reliability of this Raman band for surface mapping, see Chapter 1d). Among the two Raman bands shared by Bv and PP, the band at 1166 cm^{-1} was better resolved at very short exposure times (2 – 5 s). Therefore, we selected this Raman band for pigment depth profiling (see Chapter 1e).

Suppl. Tab. 1: Raman band assignments for Egg colour pigments, protein degradation products, and lipids. Underlined Raman shifts are represented in the colored dots in Fig. 1, and the Extended data Figs. 1, 6, and are considered diagnostic for eggshell pigments even in presence of PFPs. Italicized Raman shifts labelled with and additional asterix are used for pigment surface maps and depth profiles (see Materials and Methods).

Raman Shift	Band Assignment	Details
600	Protoporphyrin	O-C=O Bending
664	Protoporphyrin	O-C=O Bending
713	Eggshell Mineral	CO_3^{2-}
740	Protoporphyrin	CH Out-of-Plane Deformation
762	Biliverdin	CH Out-of-Plane Deformation
770	Biliverdin	CH Out-of-Plane Deformation
775	Protoporphyrin	NH Wagging
783	Biliverdin	CH Out-of-Plane Deformation
850	Biliverdin	NH Wagging
880	Biliverdin	CH_2 Out-of-Plane Wagging
891	Protoporphyrin	CH_2 Out-of-Plane Wagging
925	Biliverdin	CH_2 Out-of-Plane Wagging
931	Protoporphyrin	CH_2 Out-of-Plane Wagging
964	Biliverdin	CH Out-of-Plane Deformation
972	Biliverdin	CH_2=CH_2 Out-of-Plane Deformation
992	Protoporphyrin	CH_2=CH_2 Out-of-Plane Deformation
1000	Biliverdin	Ring Breathing
1061	Biliverdin	C-O Stretch
1086	Eggshell Mineral	CO_3^{2-}
1115	Protoporphyrin	C-N Stretch
1128	Protoporphyrin	C-N Stretch
1157	Protoporphyrin	C-N Stretch
*1166	*Protoporphyrin, Biliverdin*	*C-N Stretch*

1177	Biliverdin	C-O-C Stretch
1225	Protoporphyrin, Peptide	C-C-N Bending, C-N Stretch, N-H Bending
1251	Biliverdin, Peptide	C-C-N Bending, C-N Stretch, N-H Bending
1266	Biliverdin, Peptide	C-C-N Bending, C-N Stretch, N-H Bending
1305	Protoporphyrin	C-N Stretch, CH_3 Deformation
1333	Protoporphyrin	C-N Stretch, CH_3 Deformation
*1350	Protoporphyrin	C-N Stretch, CH_3 Deformation
1367	Protoporphyrin	CH_3 Symmetric Deformation
1383	Protoporphyrin	CH_3 Symmetric Deformation
1391	Biliverdin	CH_3 Symmetric Deformation
1407	Biliverdin	C-N Stretch
1420	Protoporphyrin	C-N Stretch
1438	Biliverdin	N-C=O Stretch
1480	Protoporphyrin	N-H Deformation
1542	Protoporphyrin	N-H Deformation
1557	Protoporphyrin, Biliverdin	C=C Stretch
1584	Protoporphyrin	C=C Stretch
1596	Biliverdin	C=C Stretch
1599	Protoporphyrin	C=C Stretch

Raman Shift	Band Assignment	Details
1650-1690	Peptide (Amide I)	C=O Stretch
1550-1600	AGE/ALE	Pyridine-like Ring Stretch
1550-1600	(Peptide)/AGE/ALE	C=C Stretch in (Metal) Imidazole Ring
1515-1520	AGE/ALE	N-H Deformation
1430-1440	Peptide	CH_3 Antisymmetric Deformation
1434-1440	(Peptide)/AGE/ALE	(Metal) Imidazole Ring Vibration
1400-1430	(Peptide)/AGE/ALE	C-N Stretch
1360-1370	Peptide	CH_3 Symmetric Deformation
1340-1352	(Peptide)/AGE/ALE	(Metal) Imidazole Ring Vibration
1230-1250	Peptide (Amide III)	C-C-N Bending, C-N Stretch, N-H Bend

1170-1180	Peptide	C-O-C Stretch
1080-1140	AGE/ALE	C-N Stretch
1050-1070	AGE/ALE	C-O Stretch
980	Peptide/AGE/ALE	CH_2=CH_2 Out-of-Plane Deformation
960	Peptide/AGE/ALE	CH Out-of-Plane Deformation
908	Peptide/AGE/ALE	CH_2 Out-of-Plane Wagging
880	Peptide/AGE/ALE	CH_2 Out-of-Plane Wagging
830-840	Peptide/AGE/ALE	NH_2 Stretch
750-790	Acid Extraction	C-Cl Stretch
650-680	Peptide/AGE/ALE	N-C=O Bend
550	Peptide	Disulfide Bridge t-g-t
520	Peptide	Disulfide Bridge g-g-t
500	Peptide	Disulfide Bridge g-g-g

Raman Shift	Band Assignment	Details
1720-1750	Lipids	C=O Stretch
1650-1660	Lipids	C=C Stretch
1440-1460	Lipids	CH_3 Antisymmetric Deformation

d. High-resolution Raman microspectroscopy point measurements

All Raman spectroscopic analyses in this study were performed with a Horiba800 LabRam Raman microspectroscope in the Department of Geology and Geophysics at Yale University. We chose a green laser with 532 nm excitation (20 mW at the sample surface). The scattered Raman light was detected by an electron multiplier charged-coupled device (EM-CCD) after being dispersed with 1800 grooves/mm grating and passed through a 100 μm entrance slit (hole size 300 μm). The spectrometer was calibrated using the first order Si band at 520.7 cm^{-1}. For the high-resolution point measurements, we accumulated six spectra in the 300-2000 cm^{-1} region for 20s exposure time each. The sample areas selected for point measurements were thoroughly cleaned with ethanol to avoid measuring surface contamination. We selected surface

areas free of sediment, with apparently intact and undamaged eggshell surfaces. Overall, we aimed for smooth eggshell surface areas or, in ornamented eggshells, planar ridge platforms, to avoid signal reduction due to unnecessary light scattering at the sample surface. In the fossil material, pigment bands were expected to occur on broad spectral shoulders produced by eggshell PFPs[26] (please see Extended data Fig. 1). In all sampled eggshells fluorescence was moderate to absent, and was reduced by adjustments of Raman hole/slit size. All spectra were obtained and despiked in Labspec 5 software, and subjected to a baseline correction and normalization based on the highest band in each spectrum using SpectraGryph 1.2 spectroscopic software. Pigment identification was based on complete band match of the diagnostic Raman pigment band subsets (see Extended data Fig. 1, and Chapter 1c, d, e).

As shown by the point-measured extant bird eggshells, PP overlying a Bv background did not pose any problem to our analytical routine, since the laser penetrated the deeper layers of the shell (see *Dromaius novaehollandiae* sample, Fig. 1). The full width half maximum values representing band width were much smaller and the bands were much narrower in the fresh chicken eggshell, which contained only PP, compared to the emu eggshell, which contained trace amounts of PP and large amounts of Bv (Extended data Fig. 1). This indicates different modes of incorporation into the eggshell. The narrow bands found for PP suggest a more ordered organization (potentially based on PP-PP interactions) whereas the broader bands for Bv indicate covalent side chain-linkage to the eggshell organic matrix (BV-protein) as a cofactor, consistent with its deposition in deeper eggshell layers.

e. Eggshell pigment surface maps

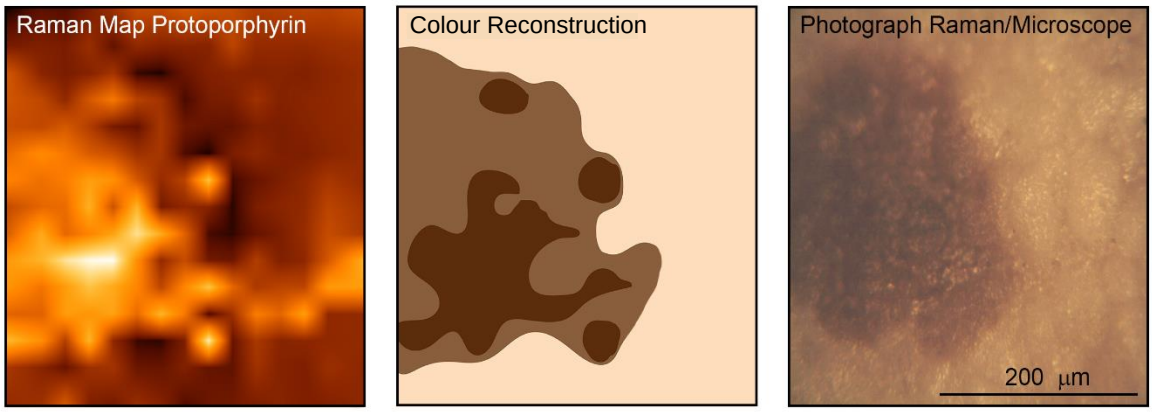

Supplementary Figure 1: Eggshell pigment map, reconstruction, and photograph of tern eggshell (YPM uncat.). A fragment of tern eggshell (*n* = 1 biologically independent sample) containing protoporphyrin spots on an almost pigment-free background (minor concentrations of protoporphyrin) were used to optimize the pigment surface maps. This pigment map was repeated three times independently with similar results. The Raman map-based reconstruction is very similar to the photograph. The Raman parameters applied are identical to those used to map protoporphyrin on the eggshell surfaces (PP-only at 1350 cm^{-1}, 2 accumulations, 5 s of exposure).

In contrast to the high-resolution point measurements, pigment surface mapping requires prior knowledge of the presence or absence of Bv and PP. Raman maps are relative, in the sense that they are normalized based on the highest concentration found in the mapped area. This means that the depicted concentration difference between a PP-rich spot on a PP-based background can appear minimal if the maximum PP-concentration does not differ much from the minimal PP-concentration.

Spots and speckles on bird eggshells are produced only by PP deposited on the outermost layer, so pigment surface maps were only obtained for PP. Since Bv is not imaged in the surface maps, the colour reconstructions and interpretations of the pigment maps combine the results from the high-resolution point measurements, and the colour patterns (Fig. 2a). If the high-resolution

point measurements suggested the presence of Bv and PP, and the surface maps produced PP spots, the overall interpretation and colour reconstructions (Fig. 2a) assumed a positive identification of Bv as the eggshell background colour. For practical reasons we chose the Raman band at 1350 cm^{-1} out of the diagnostic set of Raman bands for eggshell PP in fossils (see Chapter 1c). This band resolves well even at short exposure times and in the presence of eggshell PFPs (see Fig. 1, Chapter 1c).

We used common tern eggshells (uncatalogued YPM samples) to calibrate our mapping routine (Supplementary Fig. 1). First, spots on the eggshells were photographed using the reflected-light microscope mode of the Raman microspectroscope. Next, we selected the observed area for PP mapping, using two accumulations over 5s exposure each. Finally, we translated the obtained spectral data into normalized concentration maps for protoporphyrin, and used these pigment maps for colour pattern reconstruction. Combined with a high-resolution point measurement of the tern eggshells, the background colour was determined as only PP-based. The overall correspondence between the PP-surface map, the egg colour reconstruction, and the real egg colour (photograph) gives a measure for the reliability (high) of PP-map egg colour pattern reconstruction.

In general, only PP-positive eggshell samples were subjected to surface mapping because the relative mode of the mapping process would yield maps of background noise for pigment-negative samples. The background noise is affected by factors such as surface texture, differential preservation, and minor differences in fluorescence.

All samples found with PP (Fig. 1, 2, Supplementary Fig. 2) are likely to preserve the eggshell cuticle or remnants of it. The sample surfaces appeared very smooth and velvet-like, without any visible, larger crystals resulting from recrystallization processes. However, spots and speckles were not visible with the naked eye in most of the fossil samples.

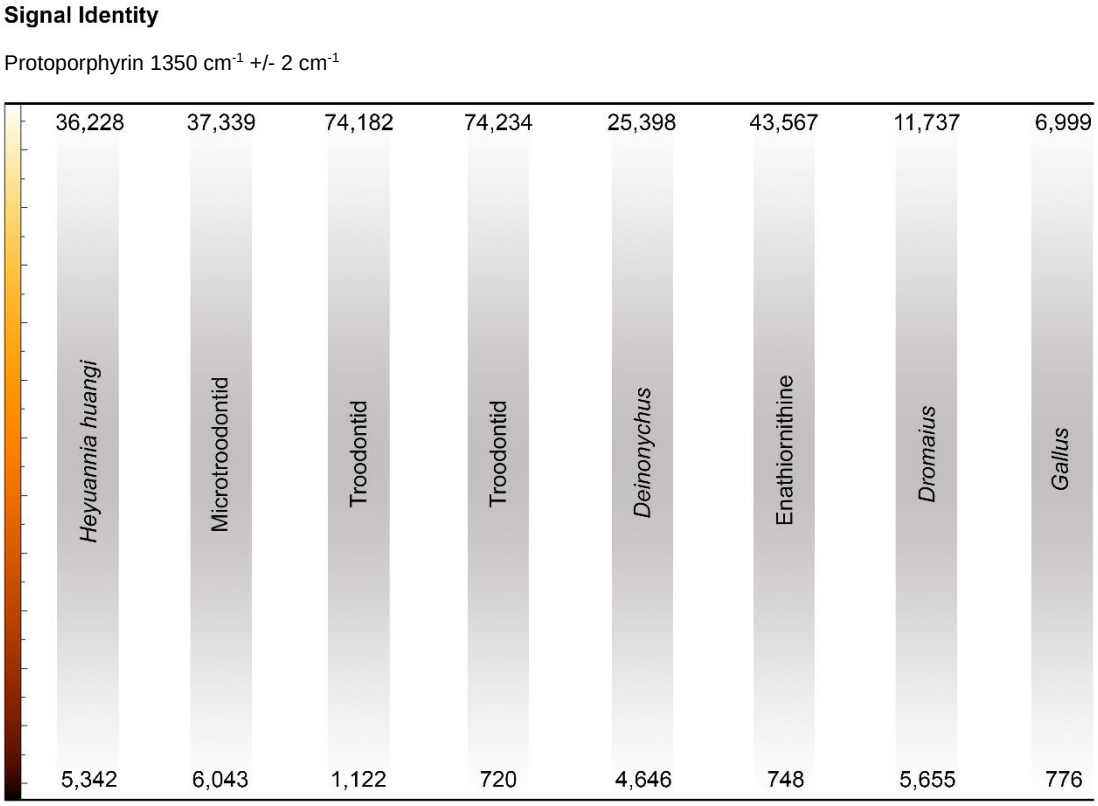

Supplementary Figure 2: Signal identity scales for the eight mapped dinosaur eggshells shown in Fig. 2.

f. Eggshell pigment depth profiles

We obtained eggshell pigment depth profiles to investigate modes of pigment deposition in non-avian and avian dinosaurs, and to validate the original nature of detected pigments. Because we were aiming to image both Bv and PP, we chose a pigment-diagnostic Raman band at 1166 cm^{-1} Raman shift (compare Supplementary Table 1 and see Chapter 1c for further explanation). This Raman band occurs on one side of a spectral shoulder related to proteinaceous matter (compare Extended data Fig. 1), which leads to an increase in signal at the eggshell membrane

or fossilized remnants of it (compare unpigmented *Alligator* eggshell, Fig. 2). Only pigment-positive samples were subjected to depth profiling, as in the case of the egg colour surface maps. Obtaining depth profiles for eggshell samples which lack pigments would yield only background-noise depth profiles. As mentioned above, background noise is affected by factors such as surface texture, differential preservation, and minor differences in fluorescence.

Pigments were assigned based on their distribution: pigments in the uppermost area were assigned to PP, and increased pigment signals in the deeper eggshell layers were assigned to Bv because PP does not extend into deeper layers. Assignments were based on combined data from the high-resolution point measurements, egg colour surface maps, and depth profiling.

The similarity in pigment stratification among all eggshells containing both Bv and PP supports the endogeneity of the detected pigments (see Fig. 2), and gives a clue about the extent of pigment elution (compare Chapter 3 on sediment composition). In combination with Extended data Fig. 4a this argues against wholesale contamination with Bv and PP metabolites of bacterial origin and corroborates our inferred endogeneity of detected dinosaur egg colour pigments. Moreover, the signal strength of the detected pigments exceeds that expected for traces of bacterial metabolites.

g. Colour reconstruction

The whole-egg colour reconstruction in Fig. 2 is based on combined evidence from the high-resolution point measurements, the pigment surface maps, and the eggshell pigment depth profiles. We offer a range of potential egg colours because organic Raman signals can only be interpreted in relative terms, and cannot be absolutely quantified. Eggshells with Bv and PP signals, and PP spots, could have had high Bv concentrations originally creating a saturated, and dark blue background colour. Alternatively they could have had low Bv concentrations, resulting in a minty *Rhea*-like background colour. However, it is not possible to reconstruct the original pigment concentrations precisely based on Raman signals, so some of the PP

potentially present could have caused a green background. Protoporphyrin spots could be lighter or darker, depending on the original amount of protoporphyrin. The diagenetic elution and potential transformation of eggshell pigments set the limits for egg colour reconstructions. Therefore, we gave three colour extremes for every fossil eggshell based on all obtained data. For more information on the difficulty of reconstructing egg colour exactly, please see the Supplemental Information in Wiemann et al. (2017)[6].

Not all samples subjected to high resolution point measurements could be used for pigment surface maps, so the egg colours/patterns presented in Fig. 2 represent an approximation based on the colour signal obtained for the Chinese troodontid and the ornithoid ratite eggshell. For the Chinese troodontid it should be noted that the spectral closeup and the eggshell net enrichment plot shown in Extended data Figs. 2 and 3 gave rise to a very weak signal which we assigned to PP based on band positions. This eggshell fragment was particularly small and characterized by a rough texture, two factors that may have reduced the spectral resolution.

h. Eggshell pigments through deep time

There is no chemical study on eggshell degradation. Macroscopic evidence of colour changes in eggs in museum collections over time suggests two pathways of pigment alteration. One pathway involves pigment browning (compare Fig. 2c) and the other pigment bleaching (compare Fig. 2c). Besides these pigment-based colour changes through time, overall browning of the eggshell was demonstrated by Wiemann et al. (2018)[26]. This browning may overprint subtle remnants of original egg colour, and is a result of oxidative transformation of proteinaceous matter during diagenesis into brown-to-black Advanced Glycoxidation End Products and Advanced Lipoxidation End Products (pigment-like protein degradation products)[26].

Assuming that parts of the pigment fraction in a fossil eggshell is transformed during diagenesis in either an oxidative or reducing fashion, the formation of significant heterogenous pigment degradation products would be expected, and only traces of unaltered pigments would remain. This proposed degradation process would be accompanied by pigment outwashing by sediment fluids, and contribute to the loss of unaltered eggshell pigments during fossilization. In addition to macroscopic colour changes in fossil eggshells, we observed that the relative signal intensities of some pigment bands are shifted (i.e. the 1327 – 1332 cm^{-1} Raman band in PP loses signal strength in fossil materials). These reduced signal strengths may represent the loss of pigment through time leaving small amounts of unaltered pigment or, more likely, they are the result of chemical alteration of certain parts of pigment molecules during fossilization.

i. Diagenetic alterations of proteinaceous matter

Eggshell pigments are stored in the waxy, lipid-rich eggshell cuticle, and in the organic scaffold of the deeper eggshell layers[23,50,51]. While PP is mainly restricted to the outermost prismatic zone and cuticle, Bv usually extends into deeper layers of the prismatic zone. Thus, pigments in fossil eggshells were originally surrounded by proteinaceous matter. During fossilization, eggshell proteinaceous matter transforms into Advanced Glycoxidation End products (AGEs) and Advanced Lipoxidation End products (ALEs)[26]. These compounds are readily detected with Raman, and cause a brownish discolouration of vertebrate hard tissues (see Supplementary Fig. 3). Chemically, AGEs and ALEs contain most of the organic functions found in eggshell pigments. In order to distinguish them we obtained a set of pigment diagnostic bands applicable to fossil eggshells with soft tissue preservation. We compared fresh avian eggshells containing Bv and PP to fossil, pigment-free dinosaur AGEs/ALEs, and selected bands diagnostic of pigments that can used to distinguish them from protein degradation products (Extended data Fig. 1).

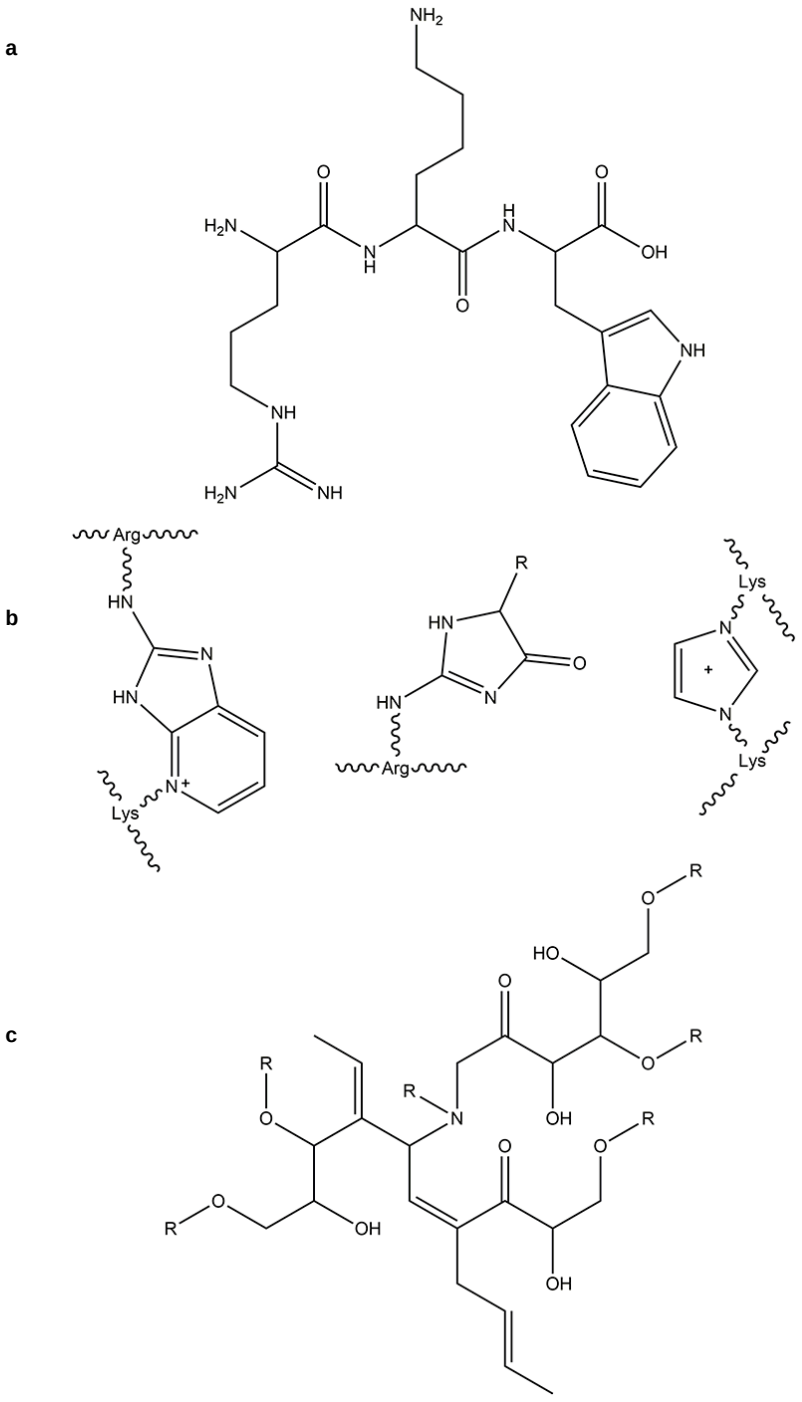

Supplementary Figure 3: Molecular structures of **a**, a tripeptide; **b**, protein fossilization products of AGE and ALE type; and **c**, an advanced melanoidin (after Wiemann et al. 2018[26])

2. List of eggshell specimens

We analyzed eggshell samples of *Alligator* and nonavian and avian dinosaurs. They range in age from Cretaceous to Recent, and came from different taphonomic and depositional environments (Supplementary Table 2).

The ornithoid ratite eggshell is not assigned to a taxon in our analysis, since the fossil is not associated with diagnostic skeletal remains; it is identified as potentially troodontid[52]. The ornithoid ratite-type organization[27,28,52] is shown in the polished vertical section across the eggshell in Supplementary Fig. 4.

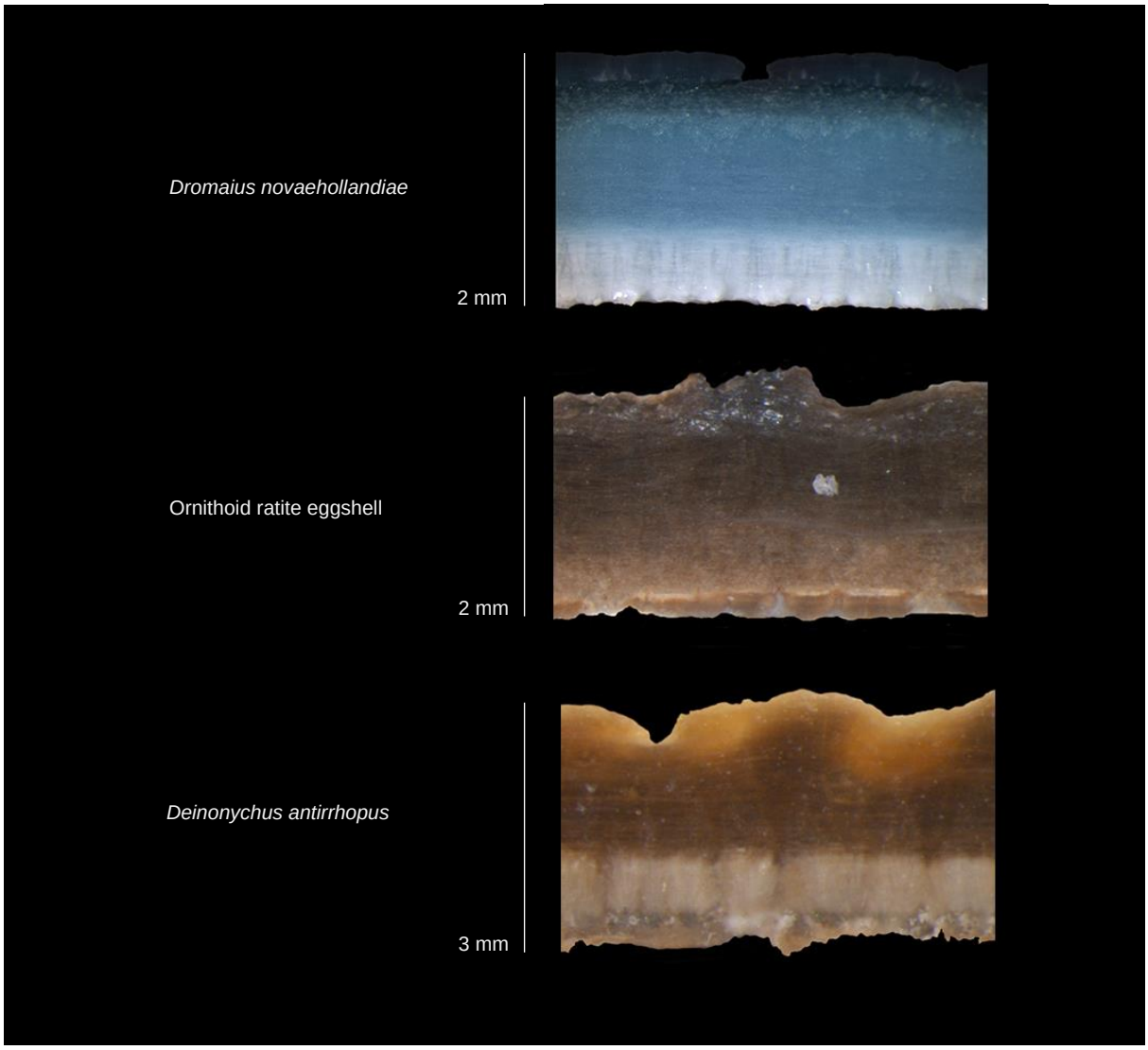

Supplementary Figure 4: Polished section across the ornithoid ratite eggshell (YPM PU 22594) from the Two Medicine Formation in Montana, US.

For the purpose of using it as control sample on false-negative signals in samples from the Two Medicine Formation, we list it (Supplementary Table 2) as unassigned (definitely eumaniraptoran), ornithoid ratite type theropod eggshells.

All other investigated eggshell specimens were taxonomically assigned in previous studies[6,8,26,29,52,53,54,55,56,57].

Supplementary Table 2: List of investigated eggshell specimens, taxa assignments, catalogue numbers, localities, and preserved colours.

Assigned Taxon	Catalogue No.	Age	Locality	Pr. Colour
Alligator mississipiensis	Uncatalogued	Quaternary	Jacksonville, FL, US	White
Maiasaura peeblesorum	YPM VP PU 023464	Cretaceous	Two Medicine Fm., Teton County, MT, US	Black
Maiasaura peeblesorum	YPM PU 22523	Cretaceous	Two Medicine Fm., Teton County, MT, US	Black
Saltasaurid	STIPB E360	Cretaceous	Sanagasta, La Rioja, Argentina	Brown
Hypselosaurus priscus	YPM PU 21158	Cretaceous	Lower Danien, Aix-en-Provence, France	Brown
Heyuannia huangi	NMNS CYN-2004-DINO-05	Cretaceous	Yuanpu Fm., Jiangxi, China	Brown
Microtroodontid	IGM 100/1323	Cretaceous	Djadochta Fm., Gobi, China	Beige
Microtroodontid	MAE 14-40	Cretaceous	Djadochta Fm., Gobi, China	Beige
Large Troodontid	YPM VP PU 023259	Cretaceous	Two Medicine Fm., Teton County, MT, US	Grey
Large Troodontid	PFMM-0014003517	Cretaceous	Chichengshan Fm., Zhejiang, China	Beige
Large Troodontid	AMNH FARB 6631	Cretaceous	Djadochta Fm., Gobi, China	Beige
Large Troodontid	IGM 100/1003	Cretaceous	Djadochta Fm., Gobi, China	Beige
Deinonychus antirrhopus	AMNH 3015	Cretaceous	Cloverly Fm., Big Horn County, MT, US	Brown
Enantiornithine	IGM 100/1339	Cretaceous	Djadochta Fm., Gobi, China	Beige
Psammornis rothschildi	ZFMK 23a:III/c/23	Quaternary	Djokran, Algeria	Black
Rhea americana	YPM ORN 24444	Quaternary	Bozeman, MT, US	Mint
Ornithoid ratite eggshells	YPM PU 22594	Cretaceous	Two Medicine Fm., Teton County, MT, US	Brown
Dromaius novaehollandiae	YPM ORN 24447	Quaternary	Bozeman, MT, US	Dark blue
Gallus domesticus	YPM ORN 23146	Quaternary	New Haven, CT, US	Brown

3. Eggshell sediment spectra validate pigment originality

We investigated all available eggshell-adherent sediment samples (see Extended data Fig. 6). Only one of the microtroodontid eggshells contained sufficient amounts of adhering sediment to be included. All sediments were treated in the same way as the eggshell samples (see Chapter 1). Raman spectra in the range 300-2000 cm^{-1} were obtained in LabSpec 5, and baselined and normalized using SpectraGryph 1.2 spectroscopic software. None of the sediment samples yielded pigment-diagnostic Raman bands (Extended data Fig. 6) compared to *Heyuannia*

huangi eggshells, which preserve both PP and Bv[6] as indicated by diagnostic Raman-based spectra. This indicates that pigments detected in the eggshell samples are of original and endogenous nature. Diagenetically outwashed eggshell pigments do not remain in the adjacent sediments. In contrast, all the sediment samples analysed contained traces of organic molecules of non-proteinaceous, non-peptide composition (Extended Data Figure 6, see Raman bands in the range 1000 – 2000 cm^{-1}).

4. Ancestral state reconstruction

No previous study includes all the taxa analysed, so we assembled a composite topology (supertree) from previously published phylogenies[8,31,32]. We used this topology, in the form of a tree manually re-drawn with Mesquite 3.4 to include the nineteen taxa analysed, as a basis for tracing the evolution of egg colour pigmentation (coded as "absent = 0" and "present = 1") using ancestral state reconstruction under parsimony (Supplementary Figure 5). No *a priori* assumption of state polarity was imposed. The result (Fig. 1 and Supplementary Fig. 5) demonstrates that egg colour had a single evolutionary origin in eumaniraptoran dinosaurs.

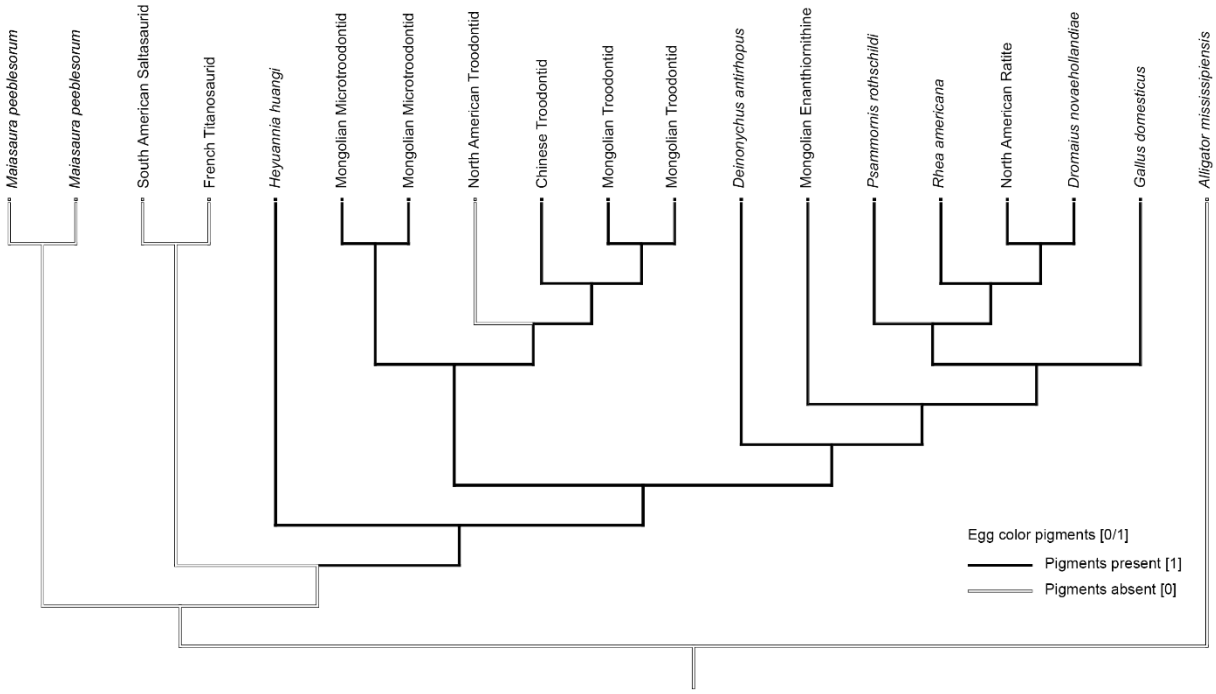

Supplementary Figure 5: Ancestral state reconstruction of egg colour in Archosauria. The phylogeny represents a pruned tree of the 19 biologically independent taxa investigated. The tree is based on previously published phylogenies[8,31,32] and was manually re-drawn in Mesquite 3.40. Egg colour is a synapomorphy of all eumaniraptorans.

5. References

33. Andrew, E. R. in *Nuclear magnetic resonance* (Cambridge University Press, 2009).

34. Dunitz, J. D. in *X-ray Analysis and the Structure of Organic Molecules* (Verlag Helvetica Chimica Acta, 1995).

35. Barnes, J. in *High performance liquid chromatography* (John Wiley & Sons, 1992).

36. Vestal, M. L. High-performance liquid chromatography-mass spectrometry. *Science* **226**, 275-281 (1984).

37. Benninghoven, A., Rudenauer, F. G. & Werner, H. W. *Secondary ion mass spectrometry: basic concepts, instrumental aspects, applications and trends* (Wiley, 1987).

38. Jurinke, C., Oeth, P. & van den Boom, D. MALDI-TOF mass spectrometry. *Mol. Biotech.* **26**, 147-163 (2004).

39. Kubiak, C., Manil, L. & Couvreur, P. Sorptive properties of antibodies onto cyanoacrylic nanoparticles. *Int. J. Pharm.* **41**, 181-187 (1988).

40. Illum, L., Jones, P. D. E., Kreuter, J., Baldwin, R. W. & Davis, S. S. Adsorption of monoclonal antibodies to polyhexylcyanoacrylate nanoparticles and subsequent immunospecific binding to tumour cells in vitro. *Int. J. Pharm.* **17**, 65-76 (1983).

41. Vistoli, G., De Maddis, D., Cipak, A., Zarkovic, N., Carini, M. & Aldini, G. Advanced glycoxidation and lipoxidation end products (AGEs and ALEs): an overview of their mechanisms of formation. *Free Rad. Res.* **47**, 3-27 (2013).

42. Colthup, N. in *Introduction to infrared and Raman spectroscopy* (Elsevier, 2012).

43. Keren, S., Zavaleta, C., Cheng, Z., de La Zerda, A., Gheysens, O. & Gambhir, S. S. Noninvasive molecular imaging of small living subjects using Raman spectroscopy. *Proc. Nat. Acad. Sci.* **105**, 5844-5849 (2008).

44. Yvon, H. J. *LabSpec 5 software*. SAS Headquarters (2010).

45. Menges, F. *Spectragryph-Optical Spectroscopy Software, version 1.0.7.* (Universität Konstanz, 2017).

46. Hammer, Ø., Harper, D. A. T. & Ryan, P. D. *PAST-Palaeontological statistics* (www. uv. es/~ pardomv/pe/2001_1/past/pastprog/past. pdf, acessado em, 2009).

47. Hu, S., Smith, K. M., & Spiro, T. G. Assignment of protoheme resonance Raman spectrum by heme labeling in myoglobin. *J. Am. Chem. Soc.* **118**, 12638-12646 (1996).

48. Hu, J. et al. Fourier-transform Raman and infrared spectroscopic analysis of novel biliverdin compounds. *Spectrochim. Acta A* **56**, 2365-2372 (2000).

49. Hu, J. et al. Fourier-transform Raman and infrared spectroscopic analysis of dipyrrinones and mesobilirubins. *Spectrochim. Acta A 57*, 2737-2743 (2001).

50. Wang, X. T. *et al*. Study of the deposition process of eggshell pigments using an improved dissolution method. *Poultry Sci.* **86**, 2236-2238 (2007).

51. Poole, H. K. Spectrophotometric identification of eggshell pigments and timing of superficial pigment deposition in the Japanese quail. *Proc. Soc. Exp. Biol. Med.* **119**, 547-551 (1965).

52. Hirsch, K. F. & Quinn, B. Eggs and eggshell fragments from the Upper Cretaceous two medicine formation of Montana. *J. Vert. Pal.* **10**, 491-511 (1990).

53. Sato, T., Cheng, Y. N., Wu, X. C., Zelenitsky, D. K. & Hsiao, Y. F. A pair of shelled eggs inside a female dinosaur. *Science* **308**, 375-375. (2005).

54. Horner, J. R. Egg clutches and embryos of two hadrosaurian dinosaurs. *J. Vert. Pal.* **19**, 607-611 (1999).

55. Grellet-Tinner, G. & Makovicky, P. A possible egg of the dromaeosaur *Deinonychus antirrhopus*: phylogenetic and biological implications. *Can. J. Earth Sci.* **43**, 705-719 (2006).

56. Varricchio, D. J., Balanoff, A. M. & Norell, M. A. Reidentification of avian embryonic remains from the Cretaceous of Mongolia. *PLoS One* **10**, e0128458 (2015).

57. Sauer, E. F. Taxonomic evidence and evolutionary interpretation of *Psammornis*. *Bonn. Zool. Beitr.* **20**, 290-310. (1969).